

Control of the Bose-Einstein Condensation of Magnons by the Spin Hall Effect


Michael Schneider^{1,*}, David Breitbach¹, Rostyslav O. Serha¹, Qi Wang², Alexander A. Serga¹,
 Andrei N. Slavin³, Vasyl S. Tiberkevich³, Björn Heinz¹, Bert Lägél¹, Thomas Brächer¹,
 Carsten Dubs⁴, Sebastian Knauer², Oleksandr V. Dobrovolskiy², Philipp Pirro¹,
 Burkard Hillebrands¹, and Andrii V. Chumak²

¹*Fachbereich Physik and Landesforschungszentrum OPTIMAS, Technische Universität Kaiserslautern,
 D-67663 Kaiserslautern, Germany*

²*Faculty of Physics, University of Vienna, A-1090 Vienna, Austria*

³*Department of Physics, Oakland University, Rochester, Michigan 48326, USA*

⁴*INNOVENT e.V. Technologieentwicklung, D-07745 Jena, Germany*

 (Received 2 March 2021; revised 22 September 2021; accepted 1 October 2021; published 2 December 2021)

Previously, it has been shown that rapid cooling of yttrium-iron-garnet–platinum nanostructures, preheated by an electric current sent through the Pt layer, leads to overpopulation of a magnon gas and to subsequent formation of a Bose-Einstein condensate (BEC) of magnons. The spin Hall effect (SHE), which creates a spin-polarized current in the Pt layer, can inject or annihilate magnons depending on the electric current and applied field orientations. Here we demonstrate that the injection or annihilation of magnons via the SHE can prevent or promote the formation of a rapid cooling-induced magnon BEC. Depending on the current polarity, a change in the BEC threshold of -8% and $+6\%$ was detected. These findings demonstrate a new method to control macroscopic quantum states, paving the way for their application in spintronic devices.

DOI: [10.1103/PhysRevLett.127.237203](https://doi.org/10.1103/PhysRevLett.127.237203)

The Bose-Einstein condensate (BEC) [1], often considered because of its exotic properties as the fifth state of matter, is formed when individual atoms [2], subatomic particles [3], or quasiparticles such as Cooper pairs [4] or quanta of molecular electric oscillations [5] coalesce into a single quantum mechanical entity existing on a macroscopic scale and described by one wave function. Emerging in various physical systems from neutron stars [6] to a droplet of liquid helium [7], this state leads to fascinating and valuable for practical use macroscopic quantum phenomena, such as superconductivity and superfluidity. Recently, novel BEC applications have been proposed, including those in the rapidly developing field of quantum computing [8–13]. In contrast to existing quantum computers, which operate at about $20\ \mu\text{K}$ [14], BEC-based computing can be performed at much higher temperatures: for example, in yttrium iron garnet ($\text{Y}_3\text{Fe}_5\text{O}_{12}$, YIG) [15], magnon condensation [16] was observed at room temperature. When using such a magnon condensate in both quasiquantum and classical nanoscale devices, the possibility to control it by magnon spintronics [17] methods via spin-polarized electric currents [18] seems particularly attractive for reducing power consumption and simplifying these devices.

The formation of a BEC can be achieved by a decrease in the temperature for real-particle systems [2,19] or in a quasiparticle system by the injection of bosons, resulting in an increase in the chemical potential. The latter has been

demonstrated experimentally for exciton polaritons [20,21], photons [22,23], or magnons [16,24–30]. In the case of magnonic systems, the injection was realized by the nuclear magnetic resonance [24,31], by the parametric pumping mechanism [16,28,29,32], allowing for the injection of a large number of magnons at a given frequency, via the spin-Seebeck effect [18] or by the mechanism of rapid cooling, as it was shown recently [33]. The method of rapid cooling utilizes a dc heating pulse and the subsequent rapid cooling of YIG/Pt nanostructures. The heating generates a high population of magnons being in thermal equilibrium with the phononic system. A rapid decrease in the phononic temperature results in the break of the equilibrium. Since the lifetime of magnons is larger than the phonon cooling rate in the experiment, an overpopulation of magnons over the whole magnon spectrum is generated. This overpopulation results in a redistribution of magnons from higher to lower energies. In this way, if the temperature of the heated YIG film is high enough and the cooling process is fast enough, the magnon chemical potential is increased to the minimal energy of the magnon system and the BEC formation process is triggered.

In the previous experiments, a Pt or Al layer was used to heat the YIG nanostructure [33]. For a Pt heater an additional generation of a spin-polarized current transverse to the YIG/Pt interface due to the spin Hall effect (SHE) is expected [34–37]. The resulting spin current is known to act on the magnetization dynamics in the YIG via the spin

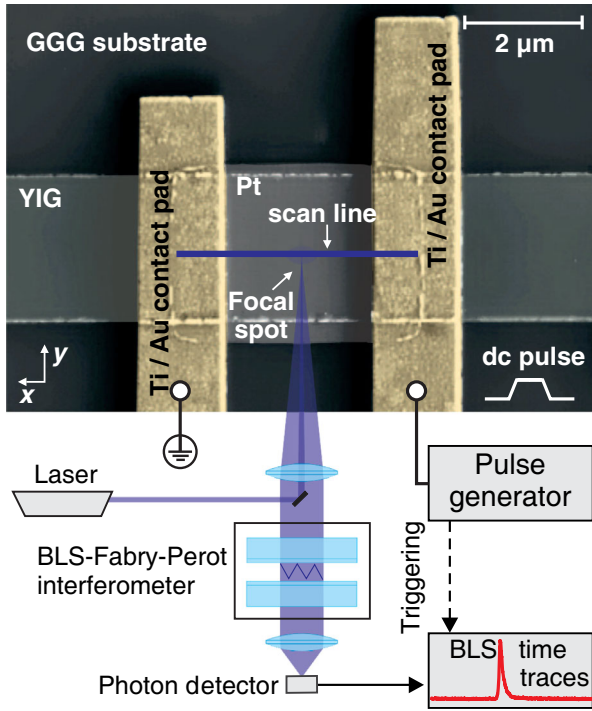


FIG. 1. Colored scanning electron microscopy image of the structure under investigation and sketch of the experimental setup. The structure consists of a $2\text{-}\mu\text{m}$ -wide and 34-nm -thick YIG stripe. A $3\text{-}\mu\text{m}$ -long and 7-nm -thick platinum heater is placed on top and contacted by Ti/Au leads separated by a distance of $2\text{ }\mu\text{m}$.

transfer torque (STT) [17,38–44]. The SHE-STT contribution, which can be checked by the variation of the current polarity with respect to the magnetization orientation in the YIG film [40], was not observed in the original experiments [33]. The reason was the large YIG film thickness of 70 nm (STT is an interface effect) and the high quality of the Pt layer grown by molecular beam epitaxy that results in a small spin Hall angle [45].

Here, we investigate a similar structure but with a smaller YIG film thickness of 34 nm [46] and with the Pt layer deposited by a sputtering technique to achieve a pronounced SHE-STT effect. Using such YIG nanostructures, we are now able to investigate the influence of the SHE-STT effect on the formation of the magnon BEC by rapid cooling. Analogously to our original studies, the experiments are conducted at room temperature. We show that the magnons annihilated or injected by the STT effect during the pulse application strongly influence the BEC formation threshold.

Figure 1 shows the structure under investigation and a sketch of the experimental setup. The structure consists of a $2\text{-}\mu\text{m}$ -wide YIG/Pt stripe ($34/7\text{ nm}$) on a (111) gadolinium gallium garnet (GGG) substrate. The YIG structure was fabricated using electron-beam lithography with subsequent argon-ion milling [47]. Afterward a $3\text{-}\mu\text{m}$ -long Pt layer was deposited on the waveguide using an

rf-sputtering technique. To establish electrical contacts to the platinum pads, Ti/Au leads ($10/150\text{ nm}$) with a distance of $2\text{ }\mu\text{m}$ between the inner edges were fabricated by electron-beam evaporation. In the presented experiments, dc pulses of a duration of $\tau_p = 100\text{ ns}$ are applied to the Pt pad. Standard ferromagnetic resonance measurements were performed on two reference pads on the same sample, one bare and one covered with platinum. These yielded Gilbert-damping constants of $\alpha_{\text{YIG}} = 1.8 \times 10^{-4}$ for the bare YIG pad and $\alpha_{\text{YIG|Pt}} = 1.7 \times 10^{-3}$ for the YIG/Pt pad, corresponding to a spin mixing conductance of $g^{\uparrow\downarrow} = 5.1 \times 10^{18}\text{ m}^{-2}$ [48]. An external field of $\mu_0\mathbf{H}_{\text{ext}} = 110\text{ mT}$ magnetizes the stripe either along its short or long axis in plane. We apply dc-current pulses to the Pt layer in order to trigger the SHE-STT-effect-based injection or annihilation of magnons and to heat up the structure. After pulse termination, the structure cools down rapidly since the GGG substrate and the Au leads act as efficient heat sinks. In such way, the experiments are conducted at room temperature and no active cooling is required. The magnetization dynamics is measured by means of Brillouin light scattering spectroscopy (BLS). A laser beam with 457 nm wavelength and $5.0 \pm 0.5\text{ mW}$ power is focused (spot size 400 nm) onto the YIG waveguide through the backside of the transparent GGG substrate, allowing one to measure below the platinum-covered YIG region [47]. The inelastically scattered light, carrying the information about the magnon intensity and frequency, is analyzed by a multipass tandem Fabry-Perot interferometer with a time resolution of about 2 ns [33,49]. The laser focus was scanned along the platinum layer between the two contact pads on a line in the middle of the stripe (see scan line indicated in Fig. 1). The resulting BLS signal was integrated along this scan line to reduce any influence of an inhomogeneous heating of the platinum region on the experimental results.

Figures 2(a)–2(c) show the measured color-coded BLS intensities (log scale) as a function of time and the BLS frequency. The amplitude of the applied dc heating pulse is $|U| = 1.5\text{ V}$, corresponding to a current density of $|j_C| = 1.6 \times 10^{12}\text{ A m}^{-2}$.

Figure 2(a) shows the reference experiment with an external field $\mu_0\mathbf{H}_{\text{ext}}$ aligned parallel to the long axis of the waveguide, parallel to the direction of the current \mathbf{j}_C ($\mu_0\mathbf{H}_{\text{ext}} \parallel \mathbf{j}_C$). In this geometry, no contribution of the SHE-STT effect is expected and the application of the current pulse only results in a Joule heating-induced increase of the YIG/Pt temperature. While the dc pulse is applied (black box in the figure), the BLS intensity decreases, as originally investigated in Ref. [50]. Further, the spectrum of thermal magnons shifts to lower frequencies due to the decrease in the saturation magnetization [15,33]. After the dc pulse is switched off at $t = 100\text{ ns}$, the heat-dissipation-induced rapid cooling triggers the formation of the BEC at the bottom of the spectrum [33].

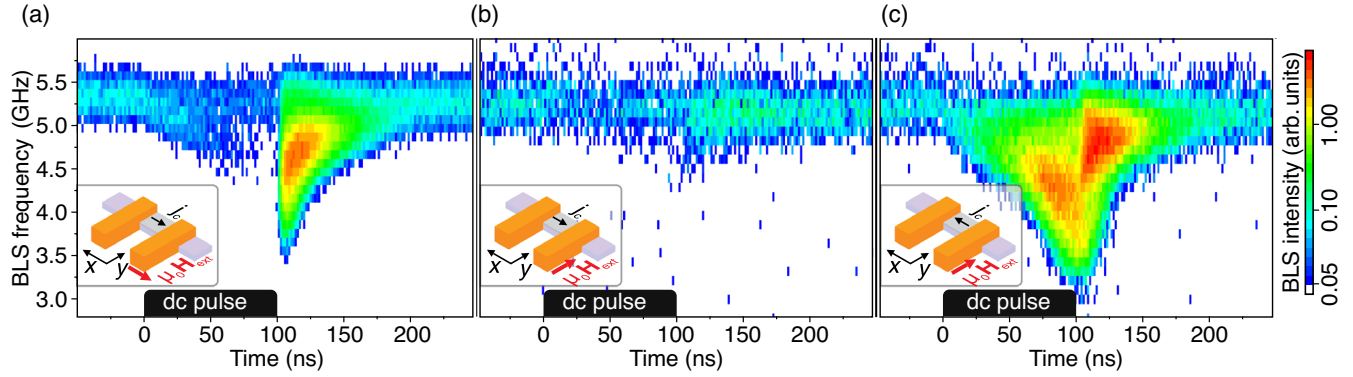


FIG. 2. BLS intensity color coded (log scale) as a function of the BLS frequency and time. The duration of the 100-ns-long heating dc pulse with an amplitude of $|U| = 1.5$ V is marked by the black boxes. (a) Current parallel to the external field, thus no contribution of the SHE-STT effect is expected. The achieved overpopulation after pulse termination due to the rapid cooling effect is sufficiently large to trigger the formation of a magnon BEC. (b) Current is perpendicular to the external field. The STT annihilates magnons during the pulse. The condensation of magnons is suppressed. (c) Reversed current direction in comparison to the situation in (b), the STT injects magnons. After the pulse is applied, the magnon BEC density is enhanced compared to the situation depicted in (a). For the exact geometries, see insets.

The BEC manifests itself as a pronounced peak in the magnon intensity. The accompanying frequency increase is due to the cooling.

The contribution of the SHE can be switched on by rotating the magnetic field by 90° , hence pointing along the short axis of the stripe [see insets in Figs. 2(b) and 2(c)], i.e., perpendicular to the direction of the dc current [40].

In this geometry, the SHE-STT contribution can be damping- or antidampinglike [34,51]. The change in the effective damping can also be described by the annihilation or injection of magnons [40] or by the change in the magnon chemical potential μ [35,39]. In the case without a STT contribution [Fig. 2(a), pulse duration of $\tau_p = 100$ ns and a voltage of $U = 1.5$ V], the magnon and the phonon system are in thermal equilibrium at the end of the dc heating pulse, and both are highly populated. The SHE-STT contribution increases or decreases the number of magnons at the end of the pulse with respect to the reference case. Thus, the SHE-STT is expected to change the BEC formation via a change of the number and distribution of excess magnons prior to the rapid cooling process [33].

Figures 2(b), and 2(c) depict the cases for magnon annihilation and injection via the SHE-STT effect, respectively. These processes can be seen in the increase or decrease of BLS intensity during the dc pulse.

The magnon annihilation process [Fig. 2(b)], in contrast to experiments on thicker YIG microstructures used previously [33], is now large enough to compensate for the rapid cooling-induced increase of the chemical potential μ , thus suppressing BEC formation.

In the case of the SHE-STT-induced magnon injection process [Fig. 2(c), $j_{C,x} < 0$, $\mu_0 \mathbf{H}_{\text{ext}} \perp \mathbf{j}_C$], the SHE-STT effect enhances the magnon redistribution, which is manifested by the even higher BLS intensity measured after the

dc pulse, compared to Fig. 2(a). For a better comparison of the three cases described above, see Supplemental Material [52] for extracted BLS spectra during and after the pulse.

Note that a purely thermal excitation of magnons takes place over the whole spectral range [Fig. 2(a)]. The subsequent decrease of the saturation magnetization leads to a decrease in the BLS intensity [50]. In contrast, for a STT injection of magnons, the BLS intensity increases [Fig. 2(c)], in spite of the heating-induced decrease of the BLS sensitivity (which does not depend on the field orientation). The reduction of the BLS sensitivity is given by the decrease in the saturation magnetization that can be treated as a thermally induced increase of the number of magnons over the whole magnon spectrum [53]. Thus, the fact that the BLS intensity in Fig. 2(c) increases rather than decreases during the heating process suggests that the SHE-STT mechanism injects magnons primarily into the low energy part of the spectrum accessible with micro-focused BLS.

The results presented in Fig. 2 show that the SHE-STT effect can control the BEC formation process via the injection or annihilation of magnons. Here, we would like to point out that the measurements presented in Figs. 2(b) and 2(c) are conducted for a fixed geometry of the field. Thus, the difference in the BEC formation after pulse termination is solely determined by the SHE-STT effect. To investigate the threshold of the BEC formation process in the presence of the SHE-STT effect, we first characterize the state of the magnon system right before the cooling takes place.

Figure 3(a) shows the inverse BLS intensity as a function of the applied voltage, now for an applied continuous dc voltage instead of a dc pulse. The linear fit of the inverse BLS intensity yields the threshold voltage for the STT-induced damping compensation [38], which is found to be

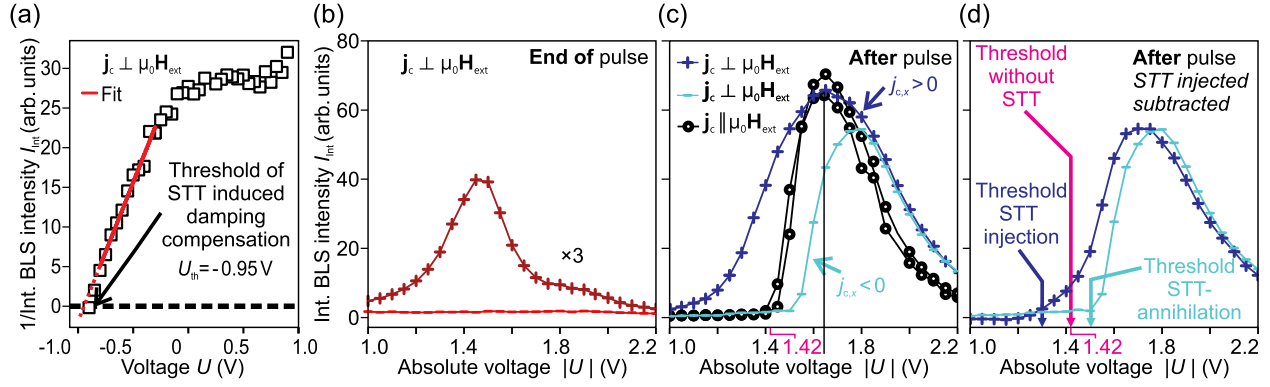


FIG. 3. (a) Inverse BLS intensity as a function of the voltage for the application of a continuous dc current. The linear fit yields a threshold for the damping compensation of $U_{th} = -0.95$ V. (b) Integrated BLS intensity at the end of the applied dc pulse (integration interval $\tau_p - 8$ ns $< t < \tau_p$) as a function of the absolute value of the voltage. The external field of $\mu_0 \mathbf{H}_{ext} = 110$ mT is aligned perpendicular to the direction of the current. The SHE-STT effect either injects (“+” sign data points) or annihilates (“-” sign data points) magnons. (c) Integrated BLS intensity after the pulse is switched off ($\tau_p < t < \tau_p + 95$ ns) as a function of the absolute value of the voltage. The blue curves correspond to the situation in (b); the black curves show the reference curve for $\mu_0 \mathbf{H}_{ext} \parallel \mathbf{j}_C$, without a SHE-STT contribution. (d) Integrated intensity as in (c), the residual signal caused by the decaying STT-injected magnons is subtracted. Because of the injection or annihilation of magnons via the STT, the thresholds are shifted with respect to the case without a SHE-STT contribution (pink line).

$U = -0.95$ V. Thus, for the voltages applied in the pulsed experiments, the SHE-STT effect compensates the damping and should lead to the formation of auto-oscillations after a sufficiently long time [51]. In the following, we limit our discussion to the voltage regime, where no auto-oscillations are triggered. However, we discuss measurements for higher voltages in the Supplemental Material [52].

Figure 3(b) shows the BLS intensity integrated over the whole frequency range shown in Fig. 2 and integrated over the last 8 ns of the applied dc pulse as a function of the voltage. This BLS intensity at the end of the pulse is corresponding to the final magnon intensity in the frequency range accessible with BLS, which is the low frequency region of the spectrum. The + sign data points correspond to the direction in which the STT effect injects magnons, the - sign data points correspond to the case when the STT effect annihilates magnons (a negative voltage corresponds to a positive current density in the x direction and results in an injection of magnons as indicated by + sign data points). We observe an increasing BLS intensity at the end of the pulse with higher voltages, indicating an increasing STT injection. After reaching its maximum at a voltage of $U = 1.45$ V, the BLS intensity decreases again, which is attributed to a decreased spin mixing conductance due to the heating [54] and a decreased BLS sensitivity at higher temperatures [50]. The decreasing BLS intensity for opposite current polarity is a superposition of the annihilation of magnons due to the SHE-STT effect and the decreasing BLS sensitivity.

In the following, the effect of the changed magnon population at the end of the pulse on the threshold voltage of the BEC formation is investigated. The applied dc pulse voltage defines the temperature increase achieved by the

Joule heating, and, therefore, it defines the number of excess magnons redistributed in the process of rapid cooling. Thus, the investigation of the BLS intensity as a function of the applied voltage yields threshold information. For the time evolution of the temperature, see the Supplemental Material [52].

Figure 3(c) shows the BLS intensity after the pulse is switched off, integrated in the time interval $\tau_p < t < \tau_p + 95$ ns. As a reference, the black curves show the integrated BLS intensities without a SHE-STT contribution ($\mu_0 \mathbf{H}_{ext} \parallel \mathbf{j}_C$). These two curves (positive and negative current polarity) show a sudden increase at a voltage of $U = 1.42$ V, which is the threshold of the BEC formation without a SHE-STT contribution. For the case of a STT annihilation (bright blue graph), a pronounced threshold at a higher voltage of $U = 1.51$ V is observed.

In the case of STT injection, the BLS intensity after termination of the pulse (dark blue curve) is the interplay of the rapid cooling-induced magnon redistribution and the (decaying) STT-injected magnons during the pulse. To investigate if these two contributions are a linear superposition or if the SHE-STT-effect-driven injection influences the redistribution process, we need to subtract the intensity originating from an exponential decay of the STT-injected magnons. This intensity can be derived as $I^{STT}(t) = I_{t=\tau_p}^{STT} \exp[-2(t - \tau_p)/\tau_m]$, where $I_{t=\tau_p}^{STT}$ is the intensity at the end of the pulse [integrated value shown in Fig. 3(b)], and τ_m is the magnon lifetime. Fitting the time evolution of the BLS intensity for the lowest voltages applied (for STT injection, without a contribution of the rapid cooling mechanism) reveals $\tau_m = 34$ ns. Thus, by using the starting intensity of the SHE-STT-effect-injected magnons we can calculate the expected magnon

intensity after the pulse if no rapid cooling process would take place. The experimental BLS intensity after the pulse with the calculated STT contribution subtracted is shown in Fig. 3(d). For $U > 1.30$ V, we find that the intensity after the end of the pulse is larger than the intensity given by the finite lifetime of the STT-injected magnons. This lowest voltage that leads to an increase of the number of magnons above the STT-injected level is identified as the threshold of the BEC formation. In summary, the shift of the BEC formation threshold is from $U = 1.42$ V down to 1.30 V or up to $U = 1.51$ V, corresponding to a relative change of -8% or $+6\%$, respectively. As we discuss in the Supplemental Material [52], a rough estimation of the SHE-STT-effect-driven excess magnon density for $U = 1.3$ V gives $n_{\text{inj}}^{\text{STT}} \approx 8 \times 10^{19} \text{ cm}^{-3}$, which is around 10% of the excess magnon density generated by the rapid-cooling mechanism $n_{\text{inj}}^{\text{RC}} \approx 6 \times 10^{20} \text{ cm}^{-3}$. To compare, the density of injected magnons in parallel parametric pumping experiments is on the order of $10^{18} - 10^{19} \text{ cm}^{-3}$ [16].

The decreasing intensity at higher voltages [$U > 1.65$ V in Fig. 3(c)] requires further investigations, but might be attributed to the increased temperature of the YIG. At the time at which the magnon BEC occurs, the YIG is not yet cooled down to room temperature. Thus, at higher voltages, the temperature at that time is increased, resulting in a decrease of the BLS sensitivity. The difference in the BLS intensity after the pulse between the case of $j_{C,x} > 0$ and $j_{C,x} < 0$ decreases with higher voltages and vanishes for the highest voltages applied. The vanishing contribution of the SHE-STT at higher voltages $U > 1.8$ V is attributed to a decreasing spin mixing conductance with higher temperatures [54].

In conclusion, we found that the SHE-STT effect injects or annihilates magnons and thus shifts the threshold values for the rapid cooling-induced magnon BEC up to 8%. Utilizing the SHE-STT effect opens up opportunities for the control (triggering or suppression) of the magnon BEC formation when the applied voltage is close to the threshold value. The comparison between the magnon populations during the application of a dc pulse for the cases with and without a SHE-STT contribution has shown that the injection of magnons primarily takes place in the low energy part of the spectrum and thus strongly promotes the formation of a rapid cooling-induced magnon BEC. These findings suggest a new way to control the formation of a magnon BEC by the polarity of the applied current, paving the way for the utilization of macroscopic quantum states in spintronic devices.

This research was funded by the European Research Council within the Starting Grant No. 678309 “MangonCircuits” and the Advanced Grant No. 694709 “SuperMagnonics,” by the Deutsche Forschungsgemeinschaft (DFG, German Research Foundation) within the Transregional Collaborative

Research Center—TRR 173–268565370 “Spin + X” (projects B01 and B04); the Project 271741898, and by the Austrian Science Fund (FWF) within the project I 4696-N. This work was supported, in part, by the U.S. Air Force Office of Scientific Research under MURI Grant No. FA9550-19-1-0307, and by the TWEED grant DARPA-PA-19-04-05-FP-001 from DARPA.

*mi_schne@rhrk.uni-kl.de

- [1] A. Einstein, Quantentheorie des einatomigen idealen Gases, Sitzungsber. Preuss. Akad. Wiss. Phys.-Math. Kl. **22**, 261 (1924).
- [2] M. H. Anderson, J. R. Ensher, M. R. Matthews, C. E. Wieman, and E. A. Cornell, Observation of Bose-Einstein condensation in a dilute atomic vapor, *Science* **269**, 198 (1995).
- [3] V. V. Begun and M. I. Gorenstein, Bose-Einstein condensation in the relativistic pion gas: Thermodynamic limit and finite size effects, *Phys. Rev. C* **77**, 064903 (2008).
- [4] L. N. Cooper, Bound electron pairs in a degenerate Fermi gas, *Phys. Rev.* **104**, 1189 (1956).
- [5] H. Fröhlich, Bose condensation of strongly excited longitudinal electric modes, *Phys. Lett.* **26A**, 402 (1968).
- [6] B. Dnil, T. Harko, and Z. Kovács, Thin accretion disks around cold Bose-Einstein condensate stars, *Eur. Phys. J. C* **75**, 203 (2015).
- [7] G. E. Volovik, *The Universe in a Helium Droplet* (Oxford University Press, New York, 2009).
- [8] K. Nakata, K. A. van Hoogdalem, P. Simon, and D. Loss, Josephson and persistent spin currents in Bose-Einstein condensates of magnons, *Phys. Rev. B* **90**, 144419 (2014).
- [9] Y. Tserkovnyak and M. Kläui, Exploiting Coherence in Nonlinear Spin-Superfluid Transport, *Phys. Rev. Lett.* **119**, 187705 (2017).
- [10] T. Byrnes, K. Wen, and Y. Yamamoto, Macroscopic quantum computation using Bose-Einstein condensates, *Phys. Rev. A* **85**, 040306(R) (2012).
- [11] S. N. Andrianov and S. A. Moiseev, Magnon qubit and quantum computing on magnon Bose-Einstein condensates, *Phys. Rev. A* **90**, 042303 (2014).
- [12] Y. Xue, I. Chestnov, E. Sedov, E. Kiktenko, A. K. Fedorov, S. Schumacher, X. Ma, and A. Kavokin, Split-ring polariton condensates as macroscopic two-level quantum systems, *Phys. Rev. Research* **3**, 013099 (2021).
- [13] S. Ghosh and T. C. H. Liew, Quantum computing with exciton-polariton condensates, *npj Quantum Inf.* **6**, 16 (2020).
- [14] F. Arute *et al.*, Quantum supremacy using a programmable superconducting processor, *Nature (London)* **574**, 505 (2019).
- [15] V. Cherepanov, I. Kolokolov, and V. L'vov, The saga of YIG: Spectra, thermodynamics, interaction and relaxation of magnons in a complex magnet, *Phys. Rep.* **229**, 81 (1993).
- [16] S. O. Demokritov, V. E. Demidov, O. Dzyapko, G. A. Melkov, A. A. Serga, B. Hillebrands, and A. N. Slavin, Bose-Einstein condensation of quasi-equilibrium magnons

- at room temperature under pumping, *Nature (London)* **443**, 430 (2006).
- [17] A. V. Chumak, V. I. Vasyuchka, A. A. Serga, and B. Hillebrands, Magnon spintronics, *Nat. Phys.* **11**, 453 (2015).
- [18] C. Safranski, I. Barsukov, H. K. Lee, T. Schneider, A. A. Jara, A. Smith, H. Chang, K. Lenz, J. Lindner, Y. Tserkovnyak, M. Wu, and I. N. Krivorotov, Spin caloritronic nano-oscillator, *Nat. Commun.* **8**, 117 (2017).
- [19] K. B. Davis, M. O. Mewes, M. R. Andrews, N. J. van Druten, D. S. Durfee, D. M. Kurn, and W. Ketterle, Bose-Einstein Condensation in a Gas of Sodium Atoms, *Phys. Rev. Lett.* **75**, 3969 (1995).
- [20] J. Kasprzak, M. Richard, S. Kundermann, A. Baas, P. Jeambrun, J. M. J. Keeling, F. M. Marchetti, M. H. Szymańska, R. André, J. L. Staehli, V. Savona, P. B. Littlewood, B. Deveaud, and S. Le Dang, Bose-Einstein condensation of exciton polaritons, *Nature (London)* **443**, 409 (2006).
- [21] G. Lerario, A. Fieramosca, F. Barachati, D. Ballarini, K. S. Daskalakis, L. Dominici, M. de Giorgi, S. A. Maier, G. Gigli, S. Kéna-Cohen, and D. Sanvitto, Room-temperature superfluidity in a polariton condensate, *Nat. Phys.* **13**, 837 (2017).
- [22] J. Klaers, J. Schmitt, F. Vewinger, and M. Weitz, Bose-Einstein condensation of photons in an optical microcavity, *Nature (London)* **468**, 545 (2010).
- [23] T. Damm, J. Schmitt, Q. Liang, D. Dung, F. Vewinger, M. Weitz, and J. Klaers, Calorimetry of a Bose-Einstein-condensed photon gas, *Nat. Commun.* **7**, 11340 (2016).
- [24] Y. M. Bunkov and G. E. Volovik, Bose-Einstein condensation of magnons in superfluid ^3He , *J. Low Temp. Phys.* **150**, 135 (2008).
- [25] T. Nikuni, M. Oshikawa, A. Oosawa, and H. Tanaka, Bose-Einstein Condensation of Dilute Magnons in TlCuCl_3 , *Phys. Rev. Lett.* **84**, 5868 (2000).
- [26] L. Yin, J. S. Xia, V. S. Zapf, N. S. Sullivan, and A. Paduan-Filho, Direct Measurement of the Bose-Einstein Condensation Universality Class in $\text{NiCl}_2 - 4\text{SC}(\text{NH}_2)_2$ at Ultralow Temperatures, *Phys. Rev. Lett.* **101**, 187205 (2008).
- [27] T. Giamarchi, C. Rüegg, and O. Tchernyshyov, Bose-Einstein condensation in magnetic insulators, *Nat. Phys.* **4**, 198 (2008).
- [28] A. A. Serga, V. S. Tiberkevich, C. W. Sandweg, V. I. Vasyuchka, D. A. Bozhko, A. V. Chumak, T. Neumann, B. Obry, G. A. Melkov, A. N. Slavin, and B. Hillebrands, Bose-Einstein condensation in an ultra-hot gas of pumped magnons, *Nat. Commun.* **5**, 3452 (2014).
- [29] D. A. Bozhko, A. A. Serga, P. Clausen, V. I. Vasyuchka, F. Heussner, G. A. Melkov, A. Pomyalov, V. S. L'vov, and B. Hillebrands, Supercurrent in a room-temperature Bose-Einstein magnon condensate, *Nat. Phys.* **12**, 1057 (2016).
- [30] S. M. Rezende, Theory of coherence in Bose-Einstein condensation phenomena in a microwave-driven interacting magnon gas, *Phys. Rev. B* **79**, 174411 (2009).
- [31] S. Autti, P. J. Heikkinen, J. T. Mäkinen, G. E. Volovik, V. V. Zavjalov, and V. B. Eltsov, AC Josephson effect between two superfluid time crystals, *Nat. Mater.* **20**, 171 (2021).
- [32] V. S. L'vov, *Wave Turbulence under Parametric Excitation: Applications to Magnetism* (Springer, Berlin, 1994).
- [33] M. Schneider *et al.*, Bose-Einstein condensation of quasi-particles by rapid cooling, *Nat. Nanotechnol.* **15**, 457 (2020).
- [34] M. Collet, X. de Milly, O. d'Allivy Kelly, V. V. Naletov, R. Bernard, P. Bortolotti, J. Ben Youssef, V. E. Demidov, S. O. Demokritov, J. L. Prieto, M. Muñoz, V. Cros, A. Anane, G. de Loubens, and O. Klein, Generation of coherent spin-wave modes in yttrium iron garnet microdiscs by spin-orbit torque, *Nat. Commun.* **7**, 10377 (2016).
- [35] L. J. Cornelissen, K. J. H. Peters, G. E. W. Bauer, R. A. Duine, and B. J. van Wees, Magnon spin transport driven by the magnon chemical potential in a magnetic insulator, *Phys. Rev. B* **94**, 014412 (2016).
- [36] L. J. Cornelissen, J. Liu, B. J. van Wees, and R. A. Duine, Spin-Current-Controlled Modulation of the Magnon Spin Conductance in a Three-Terminal Magnon Transistor, *Phys. Rev. Lett.* **120**, 097702 (2018).
- [37] M. Madami, S. Bonetti, G. Consolo, S. Tacchi, G. Carlotti, G. Gubbiotti, F. B. Mancoff, M. A. Yar, and J. Åkerman, Direct observation of a propagating spin wave induced by spin-transfer torque, *Nat. Nanotechnol.* **6**, 635 (2011).
- [38] V. E. Demidov, S. Urazhdin, E. R. J. Edwards, M. D. Stiles, R. D. McMichael, and S. O. Demokritov, Control of Magnetic Fluctuations by Spin Current, *Phys. Rev. Lett.* **107**, 107204 (2011).
- [39] V. E. Demidov, S. Urazhdin, B. Divinskiy, V. D. Bessonov, A. B. Rinkevich, V. V. Ustinov, and S. O. Demokritov, Chemical potential of quasi-equilibrium magnon gas driven by pure spin current, *Nat. Commun.* **8**, 1579 (2017).
- [40] M. Schreier, G. E. W. Bauer, V. I. Vasyuchka, J. Flipse, K. i. Uchida, J. Lotze, V. Lauer, A. V. Chumak, A. Serga, S. Daimon, T. Kikkawa, E. Saitoh, B. J. Wees, B. Hillebrands, R. Gross, and S. T. B. Goennenwein, Sign of inverse spin Hall voltages generated by ferromagnetic resonance and temperature gradients in yttrium iron garnet platinum bilayers, *J. Phys. D* **48**, 025001 (2015).
- [41] E. Saitoh, M. Ueda, H. Miyajima, and G. Tatara, Conversion of spin current into charge current at room temperature: Inverse spin-Hall effect, *Appl. Phys. Lett.* **88**, 182509 (2006).
- [42] T. Wimmer, M. Althammer, L. Liensberger, N. Vlietstra, S. Geprägs, M. Weiler, R. Gross, and H. Huebl, Spin Transport in a Magnetic Insulator with Zero Effective Damping, *Phys. Rev. Lett.* **123**, 257201 (2019).
- [43] A. Hamadeh, O. d'Allivy Kelly, C. Hahn, H. Meley, R. Bernard, A. H. Molpeceres, V. V. Naletov, M. Viret, A. Anane, V. Cros, S. O. Demokritov, J. L. Prieto, M. Muñoz, G. de Loubens, and O. Klein, Full Control of the Spin-Wave Damping in a Magnetic Insulator Using Spin-Orbit Torque, *Phys. Rev. Lett.* **113**, 197203 (2014).
- [44] E. Padrón-Hernández, A. Azevedo, and S. M. Rezende, Amplification of spin waves in yttrium iron garnet films through the spin Hall effect, *Appl. Phys. Lett.* **99**, 192511 (2011).
- [45] E. Sagasta, Y. Omori, M. Isasa, M. Gradhand, L. E. Hueso, Y. Niimi, Y. C. Otani, and F. Casanova, Tuning the spin Hall effect of Pt from the moderately dirty to the superclean regime, *Phys. Rev. B* **94**, 060412(R) (2016).
- [46] C. Dubs, O. Surzhenko, R. Thomas, J. Osten, T. Schneider, K. Lenz, J. Grenzer, R. Hübner, and E. Wendler, Low damping and microstructural perfection of sub-40 nm-thin yttrium iron garnet films grown by liquid phase epitaxy, *Phys. Rev. Mater.* **4**, 024416 (2020).

- [47] B. Heinz, T. Brächer, M. Schneider, Q. Wang, B. Lägél, A. M. Friedel, D. Breitbach, S. Steinert, T. Meyer, M. Kewenig, C. Dubs, P. Pirro, and A. V. Chumak, Propagation of spin-wave packets in individual nanosized yttrium iron garnet magnonic conduits, *Nano Lett.* **20**, 4220 (2020).
- [48] C. Du, H. Wang, P. C. Hammel, and F. Yang, $Y_3Fe_5O_{12}$ spin pumping for quantitative understanding of pure spin transport and spin Hall effect in a broad range of materials (invited), *J. Appl. Phys.* **117**, 172603 (2015).
- [49] T. Sebastian, K. Schultheiss, B. Obry, B. Hillebrands, and H. Schultheiss, Micro-focused Brillouin light scattering: Imaging spin waves at the nanoscale, *Front. Phys.* **3**, 35 (2015).
- [50] K. S. Olsson, K. An, X. Ma, S. Sullivan, V. Venu, M. Tsoi, J. Zhou, L. Shi, and X. Li, Temperature-dependent Brillouin light scattering spectra of magnons in yttrium iron garnet and permalloy, *Phys. Rev. B* **96**, 024448 (2017).
- [51] V. Lauer, M. Schneider, T. Meyer, T. Brächer, P. Pirro, B. Heinz, F. Heussner, B. Lägél, M. C. Onbasli, C. A. Ross, B. Hillebrands, and A. V. Chumak, Temporal evolution of auto-oscillations in an yttrium-iron-garnet/platinum micro-disk driven by pulsed spin Hall effect-induced spin-transfer torque, *IEEE Magn. Lett.* **8**, 1 (2017).
- [52] See Supplemental Material at <http://link.aps.org/supplemental/10.1103/PhysRevLett.127.237203> for a detailed description of the magnon spectra shown in the manuscript, magnon spectra for larger voltages and different geometries, an estimation of the elevated temperature, and a quantitative description of the magnon injection.
- [53] W. Wetling, M. G. Cottam, and J. R. Sandercock, The relation between one-magnon light scattering and the complex magneto-optic effects in YIG, *J. Phys. C* **8**, 211 (1975).
- [54] K.-i. Uchida, T. Kikkawa, A. Miura, J. Shiomi, and E. Saitoh, Quantitative Temperature Dependence of Longitudinal Spin Seebeck Effect at High Temperatures, *Phys. Rev. X* **4**, 041023 (2014).